Ultrasonic Wireless Power Transfer in Metal Structures using Frequency-Steerable Acoustic Transducers and Impedance Matching

Ultrasonic Wireless Power Transfer in Metal Structures using Frequency-Steerable Acoustic Transducers and Impedance Matching

Stefano Taccetti
ARCES - University of Bologna
40136 Bologna, Italy
stefano.taccetti2@unibo.it

Federica Zonzini
DEI - University of Bologna
40136 Bologna, Italy
federica.zonzini@unibo.it

Matteo Zauli
CIRI ICT - University of Bologna
47521 Cesena, Italy
matteo.zauli7@unibo.it

Masoud Mohammadgholiha
DEI - University of Bologna
40136 Bologna, Italy
m.mohammadgholiha@unibo.it

Lorenzo Mistral Peppi
ARCES - University of Bologna
40136 Bologna, Italy
lorenzomistral.pepp2@unibo.it

Aldo Romani
DEI/ARCES, University of Bologna
47522 Cesena, Italy
aldo.romani@unibo.it

Luca De Marchi
DEI - University of Bologna
40136 Bologna, Italy
l.demarchi@unibo.it

***Abstract*—Ultrasonic Wireless Power Transfer (UWPT) has been widely investigated in recent years as a promising solution for powering inaccessible sensor nodes in structural health monitoring (SHM) applications without affecting materials' integrity and overcoming metal shielding effect. In this work, the Frequency-Steerable Acoustic Transducer (FSAT) has been considered as an innovative device for ultrasonic guided waves-based energy transmission thanks to its directional properties. Power transmission and conversion from ultrasonic waves have been investigated, along with techniques exploiting impedance matching to ensure maximum power transfer and sufficient voltage at the receiver side. More specifically, FSAT's output impedance is measured and two impedance-matching networks are proposed and characterized: a parallel-connected inductor and a magnetic transformer. Experimental results conducted on a $1\,\mathrm{mm}$ thick aluminum plate with two FSATs bonded at a $50\,\mathrm{cm}$ distance pointed out a maximum received power value of $164\,\mu\mathrm{W}$ at $83\,\mathrm{kHz}$, with a $23\,\mathrm{V}$ peak-to-peak voltage in transmission. The received power and voltage are sufficient to energize a low-end MCU and micropower management circuits on a sensor node.**

***Index Terms*—Frequency Steerable Acoustic Transducers (FSATs), Impedance matching, Ultrasonic wireless power transfer, Energy harvesting**

I. Introduction

Structural Health Monitoring (SHM) gathers several techniques for system health diagnosis and damage identification [1]. While alleviating the electrical and geometrical constraints compared with the wired alternatives, wireless connectivity is a widespread technological solution for this kind of application However, wireless transmission is generally a power-demanding task and, therefore, energy autonomy is a fundamental requirement to ensure long-lasting sensor nodes. Energy harvesting is a promising technology to support this goal. Requirements become even stricter in metal structures, since drilling holes for supply wires can compromise structural integrity, and costs for battery replacement are unbearable [2]. In these structures, e.g., fuselages [3], chassis or pipelines [4], nondestructive evaluation techniques (NDE) are generally performed by ultrasonic guided waves (GWs), because of their ability to travel long distances with negligible attenuation [5].

For these reasons, GWs have also been studied to achieve ultrasonic wireless power transfer (UWPT) and energize inaccessible sensor nodes. In these terms, UWPT provides an alternative or additional solution to typical energy harvesting techniques, which can be affected by problems of time and space availability of the natural energy source [6], [7].

GWs-based systems are mostly implemented using piezoelectric (PZT) transducers permanently attached to the structure being inspected [8]; consequently, most of the UWPT-related studies are based on PZT arrays [2], [6], [9]. However, the integration of this technology is limited by several factors: bulky hardware instrumentation high power consumption and integration costs, as well as poor directivity. To bypass these challenges, Frequency Steerable Acoustic Transducers (FSATs) offer inherent directional capabilities that can profitably be used instead of traditional piezoelectric transducers [10]. FSATs leverage frequency-dependent spatial filtering effects, resulting in a direct relationship between the Lamb wave direction of propagation and the frequency content of the driving/received signals, hence maximizing the overall energy injected in the structure.

The UWPT-FSAT system architecture proposed in this work is shown in Fig. 1 for the representative case of a metal structure, highlighting functional blocks of the receiver and transmitter units.

This project has received funding from the ECSEL Joint Undertaking (JU) under grant agreement No 101007247. The JU receives support from the European Union's Horizon 2020 research and innovation programme and Finland, Germany, Ireland, Sweden, Italy, Austria, Iceland, Switzerland. This research was partly funded by PNRR – M4C2 – Investimento 1.3, Partenariato Esteso PE00000013 – "FAIR – Future Artificial Intelligence Research" – Spoke 8 "Pervasive AI", funded by the European Commission under the NextGeneration EU programme.

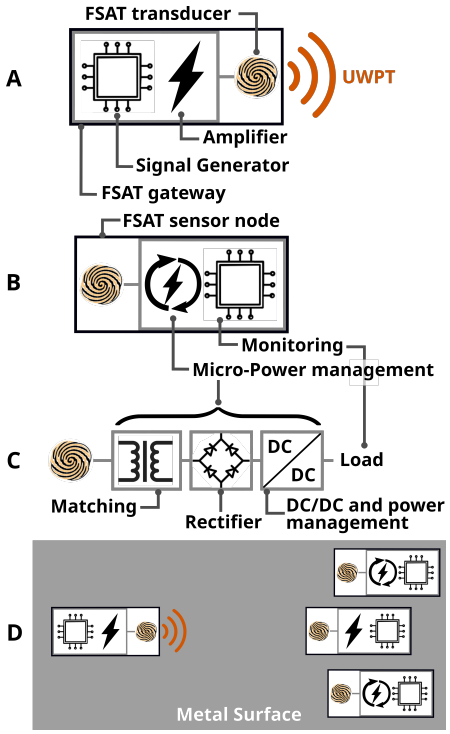

Fig. 1. System architecture and application: A) FSAT gateway (based on signal generator and power amplifier for transmission) B) FSAT sensor node (based on monitoring subsystem and micro-power management unit) C) Micro-Power management unit (based on matching network, diode rectifier and DC/DC converter) D) UWPT for metal structures monitoring application

A preliminary analysis of directional UWPT [11] with FSAT emphasizes the superior performances of FSAT over PZT-based alternatives. Proof is provided in terms of open circuit voltages at the receiver side under the same transmission conditions, i.e. the same frequency, the same peak-to-peak voltage on the electrodes, and the same distance between the transducers. Indeed, in a $83\,\mathrm{kHz}$ transmission at a $50\,\mathrm{cm}$ distance over a $1\,\mathrm{mm}$ thick aluminum plate, peak open circuit voltages of $11.32\,\mathrm{mV}$ and $134.25\,\mathrm{mV}$ were respectively measured with $2\,\mathrm{cm}$ diameter Murata PZTs and FSATs. These values are not sufficient to supply a sensor node, thus a matching network is required to boost voltage and increase received power. Impedance matching networks (IMNs), e.g., T-shaped or PI-shaped, are widely studied in ultrasonic applications [12]–[14] and they are mostly exploited to maximize power in actuation. However, this work focuses on the receiver side of the UWPT system, considering a simpler IMN to achieve, at the same time, maximum power transfer and higher voltages from the RX transducer.

The paper is structured as follows: objectives of the work are presented in section II; FSAT description together with its output impedance measurement and electrical model are presented in Section III-A, while the theory behind impedance matching is introduced in Section III-B; experimental tests of the proposed FSAT-UWPT are reported in Section IV; finally, conclusions are drawn.

II. Objectives of the Work

The final goal of the above-described system is to prove the feasibility of powering a low-power sensor node connected to the FSAT device via an efficient power management circuit (PMC), such that it can perform structural inspections in an energy-autonomous manner. To this end, two different aspects need to be evaluated at the receiver side: transducer voltage and maximum output power. By identifying suitable impedance networks, this work aims at maximizing the receiver power, while guaranteeing at the same time an adequate voltage to perform rectification and power conversion at the receiver side. Since transmitted power is significantly lower than the one typically involved in UWPT systems [2], [15], boosting the voltage amplitude in reception is fundamental to overcome the threshold voltage of rectifier diodes and the cold-start level of the DC-DC converter.

This work refers to the case of low voltages applied to the TX transducer side, and its main contributions can be summarized as follows:

1) Improvement of received power in FSAT-UWPT by matching the output impedance of the receiving transducer with two different electrical networks, one based on inductors and the second on a magnetic transformer. Transmission tests on the same experimental setup used in [11] highlighted a maximum received value of $164\,\mu\mathrm{W}$ at $83\,\mathrm{kHz}$, with $23\,\mathrm{V}$ peak-to-peak voltage in transmission and with both impedance matching networks. This corresponds to a power value is 6.56x higher than the previous work.
2) Increase of 5.68x in the output voltage in reception (maximum value of $3.23\,\mathrm{V}$) when matching the transducer's impedance with a magnetic transformer, with respect to the voltage measured with a purely inductive matching network. The gain increases to 35x when compared to a pure resistive load. A sufficient voltage at the received side is necessary to overcome the threshold of any rectifier device and the minimum input voltage of any necessary power management circuit.

III. Materials and Methods

A. Frequency-Steerable Acoustic Transducers (FSAT)

In this work, a specific type of Frequency-Steerable Acoustic Transducer (FSAT), termed as Discrete-FSAT [16], is employed for directional energy transmission. This transducer can actuate or sense Lamb waves propagating in three 60° spaced orientations, carrying three potential and distinct frequencies (between 50 and $450\,\mathrm{kHz}$) in each direction. Due to the inherent correlation between the propagation direction of ultrasonic waves and the orientation of the two transducers, a $83\,\mathrm{kHz}$ frequency was chosen, as it corresponds to the 0° direction connecting the TX and RX FSATs. The Discrete-FSAT is accessible by a couple of channels, as it is displayed by Fig 2, and, when employed for transmission, the two channels' voltages need to be in phase opposition to maximize the beam steering effect. Similarly, when the Discrete-FSAT

is employed in reception, these two channels generate two voltages again in phase opposition and the differential output, whose peak-to-peak voltage value is approximately double that of each single channel, represents the output port of the RX side for an external load. It is important to point up that this FSAT prototype was designed to work on aluminum plates and, if applied to other materials, will generate different wavelengths corresponding to different frequencies. Importantly, the electrode layout can be re-designed to retrieve the same wavelengths of the presented FSAT in case a different material would be exploited.

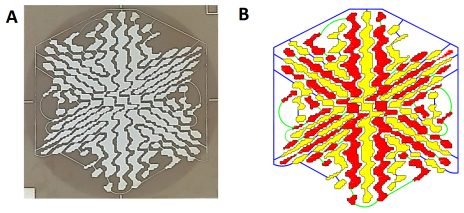

Fig. 2. Discrete-FSAT: A) fabricated device B) electrodes layout with first and second channel pads respectively in red and yellow

To study the maximum power transfer problem with FSAT, the single and differential channels' impedances were measured and modeled. Fig. 3 shows that the FSAT impedance is mainly capacitive and each single channel can be approximated with a 33 nF capacitance; on the other hand, the differential measurement, given by the series of the first and second channel is characterized by a 16.5 nF capacitance, as expected.

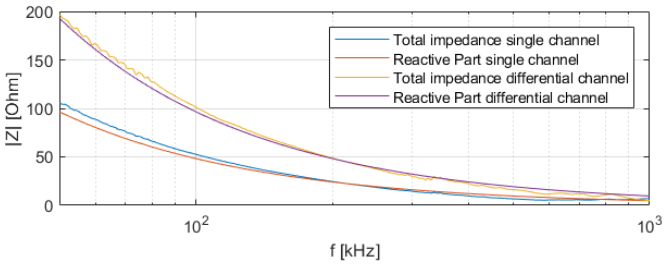

Fig. 3. Discrete-FSAT measured impedance compared with ideal capacitive impedance for transducers' single and differential channels

B. Impedance matching

Under the maximum power transfer theorem [13], a power source delivers maximum active power to an external load when the load impedance is the complex conjugate of the source impedance. An IMN is a two-port network that is designed to transform the load impedance into the source complex conjugate impedance when this condition is not met [12]. Two different kinds of IMNs, illustrated in Fig. 4, have been studied for the Discrete-FSAT differential output, respectively based on inductors and transformers, to investigate the maximum achievable output power on the receiver side of the UWPT system. Since the FSAT behavior is slightly different from the one of an ideal capacitance (Fig. 3), its output impedance has been modeled by adding a resistance R_{FSAT} in parallel with the 16.5 nF C_{FSAT}.

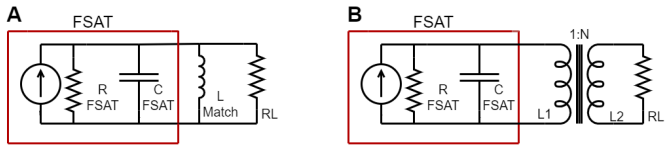

Fig. 4. Proposed Matching Network schematics: A) inductor-based B) transformer-based

1) Inductors: Since the RX FSAT can be modeled with a current generator with a capacitive and a resistive parallel branch, the simplest way to evaluate the maximum power transferred to an external resistive load is to add a parallel inductor that matches the reactive part of the source impedance (Fig. 4A). To assess this inductance value at the transmission frequency f, (1) can be used.

$$L_{match} = \frac{1}{(2\pi f)^2\ C_{FSAT}} \tag{1}$$

When power is transmitted at 83 kHz, the optimal parallel matching inductance L_{match} is equal to 223 µH considering a differential capacitance C_{FSAT} of 16.5 nF for the power source (i.e., the FSAT). Once the reactive part is compensated, the maximum active power is transferred to an external parallel resistance matching that of the FSAT:

$$R_L = R_{FSAT} \tag{2}$$

2) Transformers: A purely inductive matching network is suitable for a first experimental evaluation of the best impedance matching conditions but it is not convenient in practical applications, as voltage amplitude values are too low to allow the use of conventional rectifiers. For this reason, a second IMN, based on a magnetic transformer (Fig. 4B), is proposed to match impedance and boost external load voltage values. Considering an ideal fully-coupled transformer model with a primary inductance L_1, a secondary inductance L_2, and a purely resistive load R_L connected to the secondary winding, the transformer's primary input impedance at the transmission frequency f is given by (3).

$$Z_{in} = \frac{j2\pi f L_1 R_L}{R_L + j2\pi f L_2} \tag{3}$$

Thus, the maximum output power is achieved when (4) and (5) are met

$$R_L = N^2 R_{FSAT} \tag{4}$$

$$L_1 = \frac{1}{(2\pi f)^2\ C_{FSAT}} \tag{5}$$

where N represents transformer turn ratio ($\sqrt{L_2/L_1}$), R_{out} and C_{FSAT} indicate the output resistance and capacitance of the Discrete-FSAT differential channel, respectively, in

a Norton equivalent model. Notably, turn ratio N is the transformer's parameter that boosts load voltage, since the secondary voltage is N times the primary voltage.

IV. Experimental Validation

Circuital simulation and experimental tests were carried out to validate impedance matching theoretical results. To simplify the analysis, a specific propagation direction (corresponding to a specific transmission frequency enabled by the FSAT device) was chosen and a single value of the peak-to-peak voltage on the transmitter side was considered.

A. Experimental Setup

Experimental tests were carried out on a square aluminum plate with a length of 1 m and a thickness of 1 mm, on which two Discrete-FSATs are bonded at a distance of 50 cm. At the transmitter side, a function generator (AFG31000, Tektronix) was used for generating continuous sinusoidal signals at 83 kHz and two power amplifiers [17], one for each transmission channel, were introduced to reach a maximum voltage of 23 V peak-to-peak. Voltages and currents on an external load resistor at the receiver side were measured by using digital multimeters (Agilent 34401A, and Keithley DMM7510). Fig. 5 shows the experimental setup used for the Discrete-FSAT-based UWPT system testing, with transmitting and receiving transducers bonded on the aluminum plate and external circuitry mounted on a breadboard.

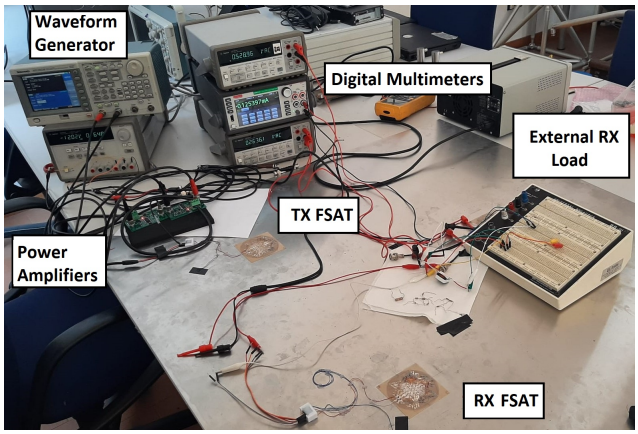

Fig. 5. Experimental setup: Discrete-FSAT bonded on the 1 mm thick aluminum plate at a distance of 50 cm along the 0° direction, electronic testing equipment and passive RX load on breadboard

B. Inductor tests

Active power measurements were carried out to validate the theoretical results of inductive IMN at continuous 83 kHz transmissions. The root-mean-square (RMS) voltage on different load resistors was measured at the receiver side and active transferred power was determined using (6). Resistance values ranging between 10 Ω and 33 kΩ from the E12 series were applied without any matching network and with matching inductances of 125 μH, 220 μH, and 560 μH.

$$P = \frac{{V_{load\ rms}}^2}{R_{load}} \tag{6}$$

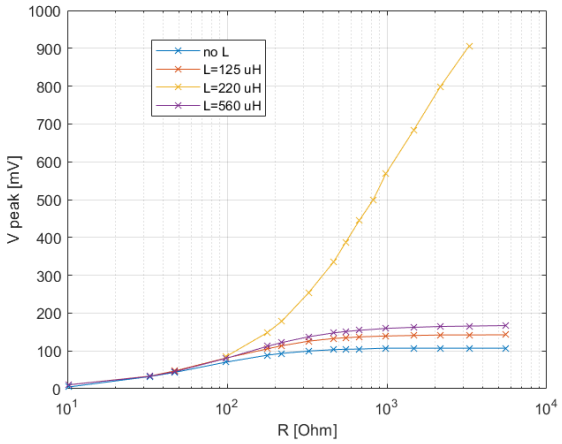

Fig. 6. Measured voltage amplitudes on the external RX load at 83 kHz with purely inductive IMNs

Fig. 7 shows the active power values from these measurements, revealing the great improvement given by the 220 µH parallel inductance, coherently with (1). Fig. 8 compares LTSpice simulation and test results without any IMN and with the optimal inductive matching condition. In these tests, the resistive load was progressively increased starting from 10 Ω until the achievement of the power peak value for each of the four configurations. For this reason, the number of resistive combinations explored for the various inductive solutions changes, depending on how rapidly the maximum peak values are reached. Despite some discrepancies due to measurement conditions, experiments validated the theoretical hypothesis, pointing out a maximum output power of 164 µW with a load resistance of 1 kΩ and a 220 µH parallel inductor, whereas a maximum of 25 µW, 6.56x lower, without any parallel inductor and a load resistance of 100 Ω. Fig. 6 shows that voltages at the RX output port exhibited maximum values of hundreds of mV, even in the optimal matching condition and in the maximum power point. Since these values are comparable with the forward voltage drop of diode rectifiers, conversion efficiency would be impaired. Then, a different matching network needs to be chosen to design a power management circuit.

C. Transformer tests

Transformer matching was considered to both extract the maximum active power and to boost voltage values on the load, in the perspective of overcoming rectifier diode thresholds and reaching an output DC voltage compatible with the cold-start of a DC-DC converter. Ten commercial transformers for switching converters with different primary inductances and different magnetic cores, gapped and ungapped, were chosen to validate (4), preferring a maximum turn ratio of 1:5 in order not to excessively scale down the secondary output current. RMS voltages on the secondary winding were measured with several resistive loads estimating the active power with (6) and progressively increasing resistance value until the achievement of the power peak value, as it was performed

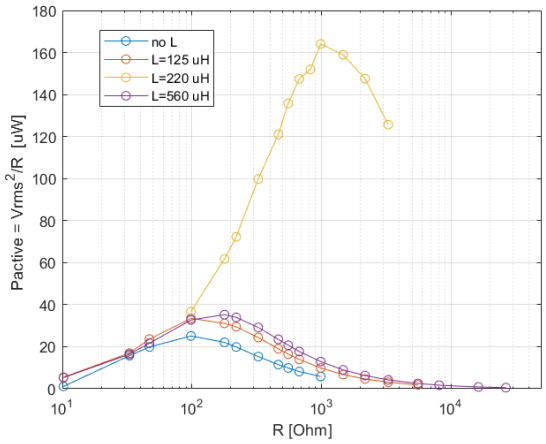

Fig. 7. Measured active power delivered to external RX load with purely inductive IMNs at 83 kHz

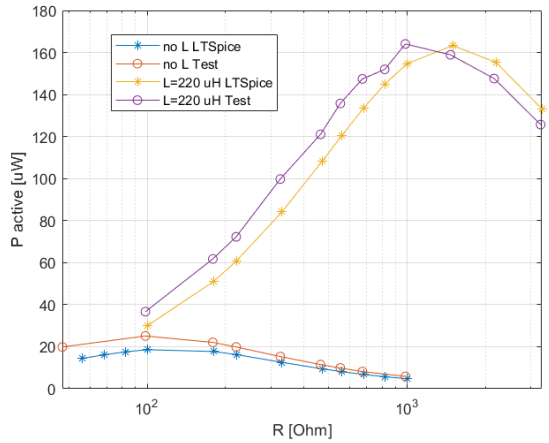

Fig. 8. Measured and simulated active power delivered to external RX load without any IMN and with the optimal purely inductive IMN at 83 kHz

with inductive IMNs. Table I summarizes the parameters of the off-the-shelf transformers used in these tests, e.g. turn ratio N and primary inductance, and maximum output power measured with the optimal load resistance R_{opt} on the secondary winding. It points out that the right choice of the transformer deeply influences the system power transfer efficiency, as the received power falls down when the transformer's input impedance is not able to match the FSAT's output one. Fig. 10 and 9 show the voltage and power measured on the secondary winding of each commercial transformer as a function of the load resistance, respectively.

Table I and Figs. 9, 10 verify the transformer-based IMNs theoretical hypotheses. Indeed, it was possible to identify a commercial device, the VPH1-1400-R by Eaton Versa-Pac series (measured primary inductance of 210 µH) able to match the FSAT output impedance and provide to the external load the same maximum power achievable with the optimal inductive IMN. Furthermore, the load resistance value that allows reaching this result is in the [22-33] kΩ range, as it

TABLE I
TRANSFORMER TEST RESULTS

Product	N	$L_{primary}$ [µH]	P_{max} [µW]	R_{opt} [kΩ]
VPH1-1400-R	5	201.6 ± 30%	161	32.5
VPH5-1200-R	5	173 ± 30%	148	21.8
749196101	5	198.6 ± 30%	75	14.7
749196108	5	224.6 ± 30%	59	8.20
750032051	5	20 ± 10%	6	0.68
750315839	5	40 ± 10%	6	0.82
749196201	5	140 ± 30%	53	8.20
750317828	4.43	206 ± 30%	53	5.60
750343725	3.9	250 ± 30%	44	3.30
750311692	5	80 ± 10%	14	1.50

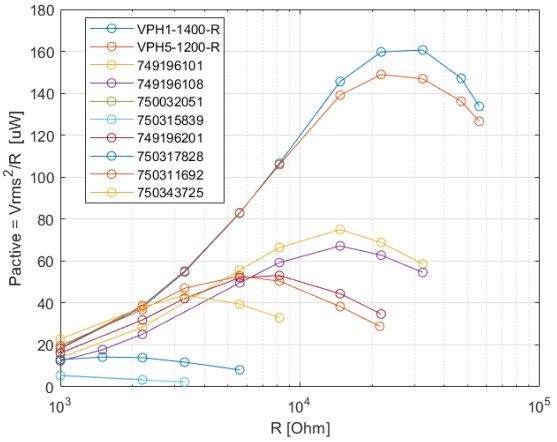

Fig. 9. Measured active power delivered by transformers to external RX load on secondary winding at 83 kHz

is displayed in Fig. 9. This result is consistent with (4) since the FSAT differential output resistance is about 1 kΩ (Fig. 8) for the transformer turn ratio of 5. While the load voltage peak in the maximum power point reached 569 mV with the 220 µH matching inductor, the VPH1-1400-R transformer provided 3.23 V, which is 5.68x higher.

D. Discussion

Almost the same maximum power value of 164 µW was measured both with a 220 µH parallel inductor and the commercial transformer VPH1-1400-R, connecting load resistances respectively of 1 kΩ and 32.5 kΩ. Moreover, this maximum power value matches the one obtained from LTSpice simulations with a 1% accuracy. It has to be mentioned that the losses introduced by necessary elements like rectifiers and power management circuits may reduce the power available for the load. However, despite this, with the reported power and voltage levels, an ultra-low-power MCU, e.g. a device from the STM32L0, STM32L4, or PIC16 families, can still be powered by a micropower DC/DC converter with voltage regulation and maximum power point tracking capabilities. It is worth noting that this is possible with a relatively low voltage applied to the TX transducers, whose impedance is not matched to the pulser output one. Furthermore, this result

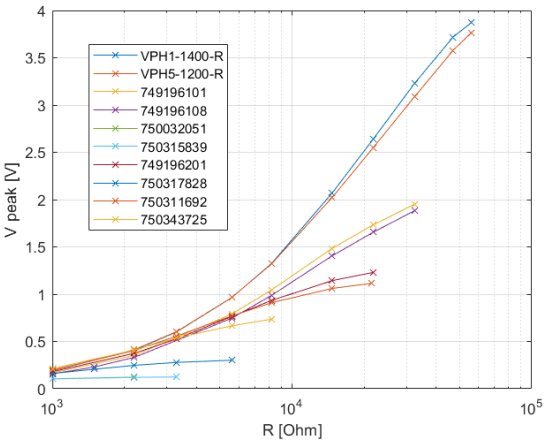

Fig. 10. Measured voltage amplitudes on the RX load on transformers' secondary winding at 83 kHz.

is achieved using simple wiring and electronic components, both for the TX and RX side, as the impedance matching is achieved by a single component and the beam focusing effect by a single transducer. These microcontrollers offer ultra-low power consumption, reaching as low as 195 nA in sleep mode and up to $28\,\mu\mathrm{A/MHz}$ in low-power run mode, hence requiring power in the order of nW to start up. The measured power of 164 µW could be sufficient to ensure the above-mentioned power-independent smart sensor functionalities.

V. Conclusions and Future Works

In this work, the problem of maximum power extraction from a directional discrete FSAT transducer was studied for UWPT applications. A 23 V peak-to-peak 83 kHz continuous sinusoidal signal was applied to each channel of the transmitting device and the receiving FSAT output power was evaluated with different loads. Two reactive networks, respectively based on a single inductor and on a transformer, were considered to match the output capacitance of the differential FSAT channel and the load resistance was tuned to reach the maximum power transfer condition. A peak power value of 164 µW, 6.56 times higher than the maximum achievable without any IMN, was measured both with a 220 µH matching inductor and the commercial transformer VPH1-1400-R, respectively, connecting a load resistance of 1 kΩ and 32.5 kΩ. Furthermore, the load voltage peak obtained with the transformer in the maximum power point is 3.23 V, 5.68x higher than the one measured with the purely inductive matching network. Based on these results, in future works, a rectifier and a low-power DC-DC converter for PMC will be included in the design, as well as one of the above-mentioned ultra-low power MCUs.

References

[1] Prateek Asthana, Jim Harkin, and Mike Hayes. Autonomous wireless sensor system design for structural health monitoring application. In *2022 IEEE Zooming Innovation in Consumer Technologies Conference (ZINC)*, pages 7–10, 2022.

[2] Yunfei Xu, Yongshun Sun, Jian Tang, Chao Wei, Xiaoxi Ding, and Wenbin Huang. A lamb waves-based wireless power transmission system for powering iot sensor nodes. *Smart Materials and Structures*, 31(10):105009, aug 2022.

[3] Guillaume Ferin, Yuvashankar Muralidharan, Naoufal Mesbah, Pascal Chatain, Claire Bantignies, Hung Le Khanh, Etienne Flesch, and An Nguyen-Dinh. Smart autonomous wireless acoustic sensors for aeronautical shm applications. In *2015 IEEE International Ultrasonics Symposium (IUS)*, pages 1–4, 2015.

[4] Abdulfattah Obeid, Fatma Karray, Wassim Jmal, Mohamed Abid, Syed Manzoor Qasim, and Mohammed Bensaleh. Toward realisation of wireless sensor network based water pipeline monitoring systems: A comprehensive review of techniques and platforms. *IET Science Measurement ? Technology*, 10, 01 2016.

[5] Marco Dibiase, Masoud Mohammadgholiha, and Luca De Marchi. Optimal array design and directive sensors for guided waves doa estimation. *Sensors*, 22(3):780, 2022.

[6] Aleksander Kural, Rhys Pullin, Karen Holford, Jonathan Lees, Jack Naylon, Christophe Paget, and Carol Featherston. Design and characterization of an ultrasonic lamb wave power delivery system. *IEEE Transactions on Ultrasonics Ferroelectrics and Frequency Control*, 60, 05 2013.

[7] Victor Farm-Guoo Tseng, Sarah S. Bedair, Joshua J. Radice, Trevon E. Drummond, and Nathan Lazarus. Ultrasonic lamb waves for wireless power transfer. *IEEE Transactions on Ultrasonics, Ferroelectrics, and Frequency Control*, 67(3):664–670, 2020.

[8] Lingyu Yu and Victor Giurgiutiu. In situ 2-d piezoelectric wafer active sensors arrays for guided wave damage detection. *Ultrasonics*, 48(2):117–134, 2008.

[9] Victor Farm-Guoo Tseng, Sarah S. Bedair, and Nathan Lazarus. Acoustic power transfer and communication with a wireless sensor embedded within metal. *IEEE Sensors Journal*, 18(13):5550–5558, 2018.

[10] Masoud Mohammadgholiha, Antonio Palermo, Nicola Testoni, Jochen Moll, and Luca De Marchi. Finite element modeling and experimental characterization of piezoceramic frequency steerable acoustic transducers. *IEEE Sensors Journal*, 22(14):13958–13970, 2022.

[11] Masoud Mohammadgholiha, Stefano Taccetti, and Luca De Marchi. Enabling directional frequency-selective power transmission in ultrasonic guided wave inspections. In *2024 IEEE South Asian Ultrasonics Symposium*, 2024. Accepted for publication.

[12] M. Garcia-Rodriguez, Javier García-Álvarez, Yasmin Yanez, Miguel Garcia-Hernandez, Jordi Salazar, A. Turo, and Juan Antonio Chávez Domínguez. Low cost matching network for ultrasonic transducers. *Physics Procedia*, 3:1025–1031, 01 2010.

[13] Haiying Huang and Daniel Paramo. Broadband electrical impedance matching for piezoelectric ultrasound transducers. *IEEE Transactions on Ultrasonics, Ferroelectrics, and Frequency Control*, 58(12):2699–2707, 2011.

[14] Vivek T. Rathod. A review of electric impedance matching techniques for piezoelectric sensors, actuators and transducers. *Electronics*, 8(2), 2019.

[15] Yongshun Sun, Yunfei Xu, Wei Li, Quanchang Li, Xiaoxi Ding, and Wenbin Huang. A lamb waves based ultrasonic system for the simultaneous data communication, defect inspection, and power transmission. *IEEE Transactions on Ultrasonics, Ferroelectrics, and Frequency Control*, 68(10):3192–3203, 2021.

[16] Masoud Mohammadgholiha, Federica Zonzini, Jochen Moll, and Luca De Marchi. Directional multifrequency guided waves communications using discrete frequency-steerable acoustic transducers. *IEEE Transactions on Ultrasonics, Ferroelectrics, and Frequency Control*, 70(11):1494–1505, 2023.

[17] Stefano Taccetti, Lorenzo Mistral Peppi, Federica Zonzini, Masoud Mohammadgholiha, Matteo Zauli, and Luca De Marchi. Design of a novel pulser for frequency selective-based power and data transmission. In *2023 IEEE International Workshop on Metrology for Automotive (MetroAutomotive)*, pages 83–87, 2023.